SPT-SLIM Electronics Rack and Detector Forecasting

Achintya Krishnan
2022 SIST Internship: Final Report
(Dated: August 12, 2022)

SPT-SLIM is an upcoming line intensity mapping (LIM) experiment on the South Pole Telescope (SPT) planned for the austral summer of 2023-2024. The readout and control electronics of the experiment will be housed within the comoving SPT cabin. The SPT-SLIM electronics rack is to be mounted to the interior walls of the cabin and house said electronics. I describe the design requirements in section II and provide an overview of the design in section III. Section IV details the testing performed to ensure that the specified criteria are met, while section V discusses the project status and upcoming action items. I then analyze the microwave kinetic inductance (MKID) detector arrays of SPT-SLIM. Its most recent signal-to-noise ratio (SNR) predictions are now outdated due to changes in the experimental configuration. Section VI will present efforts to update this SNR model such that it better reflects the current experimental design.

CONTENTS

I. BACKGROUND

A. SPT

The South Pole Telescope (SPT) is a ground-based telescope located at Amundsen-Scott South Pole Station in Antarctica. The telescope consists of a 10-meter diameter primary mirror which focuses incident light onto detectors housed within the comoving SPT cabin, as shown in Figure 1. SPT makes cosmic microwave background (CMB) measurements at mm-wavelengths. It began observation in 2007 with SPT-SZ, which ran until 2011, and investigated the angular power spectrum in temperature of the CMB. This experiment also probed the Sunyaev-Zel'dovich (SZ) effect—a frequency distortion in the CMB due to inverse Compton scattering of CMB photons by matter. SPTpol followed SPT-SZ from 2012-2016 and added polarization measurement capabilities—therefore allowing for a calculation of the CMB angular power spectrum in polarization [12]. SPT-3G commenced operations in 2017 and is still running today. Its design involved a complete overhaul of SPTpol's optical system, resulting in SPT-3G having 10 times as many detectors and pixels sensitive to 3 different frequency bands (95 GHz, 150 GHz, and 220 GHz) [11].

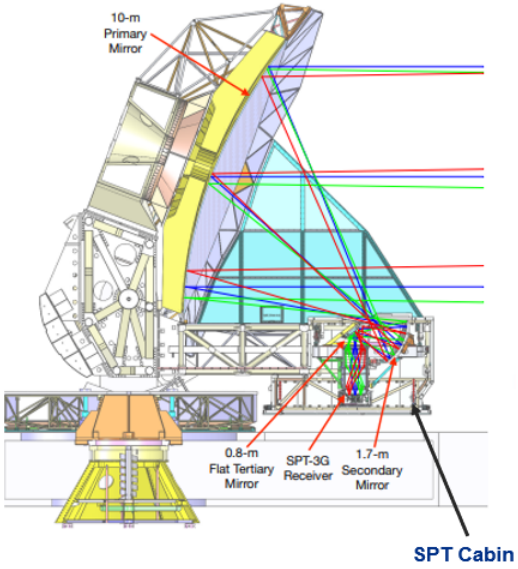

FIG. 1. SPT 10-meter diameter primary mirror focues incident light onto detectors within the comoving SPT cabin [11]

Currently, SPT-3G employs superconducting transition edge sensor (TES) bolometers [11]. SPT-3G+, which plans to replace SPT-3G in approximately 2025, and SPT-SLIM, targeted for deployment at SPT in the austral summer of 2023-2024, will transition to superconducting microwave kinetic inductance (MKID) detector arrays [3, 7].

B. Line Intensity Mapping (LIM)

Line intensity mapping (LIM) involves measuring emission from a redshifted atomic or molecular line, both spatially on the sky and spectrally to determine its redshift. This yields a 3-D mapping of large-scale structure (LSS) [7], which can be used to further constrain multiple parameters in the ΛCDM model of cosmology (e.g., sum of neutrino mass states, expansion parameters, etc.) [4]. While observing redshifts to ascertain cosmological distances has long been used, the uniqueness of LIM arises from its measurement of the microwave portion of the spectrum, large survey area, and specific application to mapping LSS. Numerous experiments—with different choices of tracer atom or molecule (e.g., Hydrogen, CO, CII, etc.)—are recently underway or upcoming [4].

The main advantages of LIM over competitors such as galaxy surveys are primarily threefold. First, it can theoretically detect higher-redshift sources [4]. For example, it has been proposed that LIM of the 21cm line of Hydrogen can be used to observe the universe during the Dark Ages ($\approx 1100 < z < 30$) [6]. Additionally, LIM is more efficient in measuring moderately high redshifts ($\approx 2 < z < 6$). Finally, this relatively new methodology has potential to unearth new science. Typically, galaxy surveys observe in the optical (or IR) range of the spectrum and therefore

utilize different tracers of the underlying matter distribution. LIM probing the microwave regime should produce a complementary dataset potentially containing undiscovered scientific truths [7].

C. SPT-SLIM

The South Pole Telescope Summertime Line Intensity Mapper (SPT-SLIM) is an upcoming LIM experiment on SPT planned for the austral summer of 2023-2024. It will target CO $J \to J-1$ rotational transition lines redshifted to between 118-183 GHz. CO is commonly found in dense molecular clouds such as star formation sites and therefore serves as a useful tracer of matter [7]. The aforementioned observation frequency range is convenient due to its close overlap with the 150 GHz observation band of SPT-3G [11].

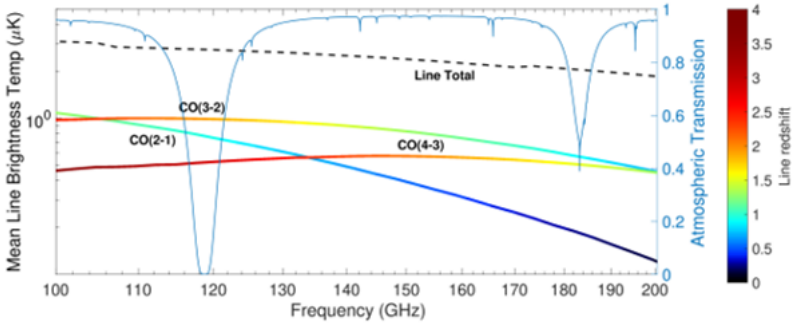

FIG. 2. Spectral lines targeted by SPT-SLIM, which will observe from 120-180 GHz. Shown are the model predictions for the brightness temperature of CO(2-1), CO(3-2), and CO(4-3), their sum total (dashed black), and median atmospheric transmission during the South Pole summer (thin blue). The colors correspond to the observed redshifts of the lines [7].

SPT-SLIM aims to serve as a proof of concept for future LIM experiments. For instance, SPT-SLIM aspires to validate on-chip spectrometer technology by demonstrating its compatibility with existing CMB telescopes and optics, applicability to mm-wave LIM [7], and scalability from single-pixel systems up to those on the order of a large array [1]. Furthermore, LIM rising to prominence only recently means that the qualities of various tracer choices are relatively unexplored. SPT-SLIM seeks to help remedy this by analyzing the advantages and disadvantages of employing CO as the tracer [7].

SPT-SLIM will be utilizing on-chip spectrometers with spectral resolutions given by $R = \frac{\lambda}{\Delta\lambda} = 300$ [7]. This corresponds to a bandwidth of 0.5 GHz for an observation band centered at 150 GHz. Each filter channel will be coupled to an MKID detector [1]. The detector arrays will fall within the SPT-SLIM cryostat, as shown in Figure 3. A pulse-tube cooler (PTC) is used to cool the 50K and 3K stages of the cryostat. Cooling beyond this will be performed by an adiabatic demagnetization regrigerator (ADR), bringing the focal plane down to 100 mK [7].

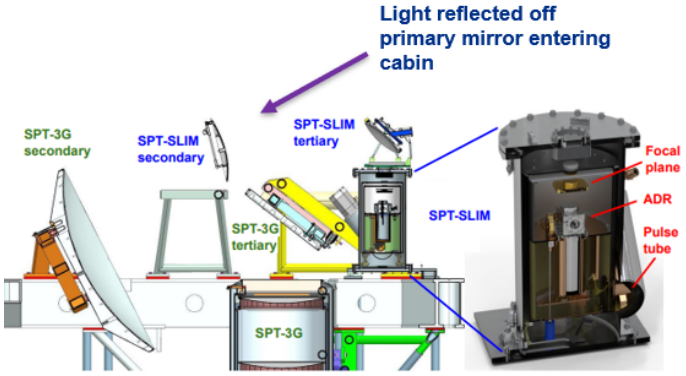

FIG. 3. Prototype mirror configuration within the SPT cabin. The focal plane, which contains SPT-SLIM's MKID detector arrays, is located within the SPT-SLIM cryostat and cooled to 100 mK. [7].

II. ELECTRONICS RACK: DESIGN REQUIREMENTS

A. Overview, Purpose, and Location

SPT-SLIM instrumentation will need various electronics to be run. For example, the ADR magnet receives current from the Lakeshore 625. Recycling of the former is regulated by the HPD1510 CryoJunction, which also controls the ADR heat switch. The readout electronics—known as iceboards—will need a power supply, cooling fans, and mini-crates for storage, while the rack mount control computer is responsible for cryostat operation. These components, along with the additional ones listed in Table I, must be securely stored within the comoving cabin. To accomplish this, it is necessary that they be housed within a specialized electronics rack. The purpose of this project is to design, fabricate, and install such a structure in the SPT cabin.

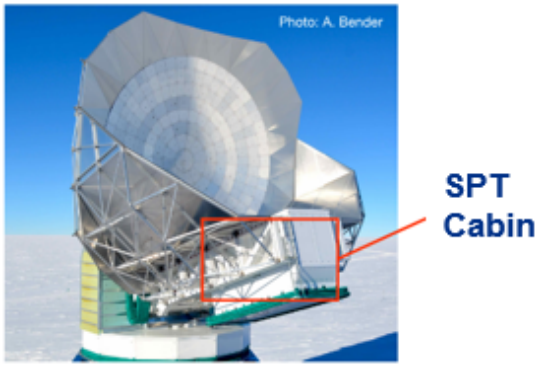

FIG. 4. External view of SPT and its cabin [1]

Component Name	Component Height (Rack Units)	Component Mass (kg)
HPD 1510 CryoJunction	2	4
Rack Mount Control Computer	1	2
Moxa Nport 5650-8 Server	1	2.3
Lakeshore 372 Resistance Bridge	2	6.8
Lakeshore 218 Diode Thermometer Readout	2	3
3x Iceboard Mini-Crates	9	6
Power Supply for Iceboards (Keysight N5744A)	1	7
Fans for Iceboards	1	N/A
Cisco CBS250-24T-4G-NA Ethernet Switch	1	2.6
Power Supply for LNAs	1	N/A
Lakeshore 625 (ADR Magnet Power Supply)	4	27.2
PTC Linear Driver	3	6.3
Uninterruptable Power Supply (UPS)	4	61.4
APC AP7900B Network-Controlled Switch	1	2.3
Total	33	130.9

TABLE I. List of electronics components to be stored in the SPT-SLIM electronics rack along with their heights and masses.

B. Design Constraints

In particular, the SPT-SLIM electronics rack must satisfy the following 3 constraints:

1. Be compact, since the cabin interior is relatively cramped.
2. Support the combined mass of itself and all electronics.
3. Maintain a stable attachment to the cabin's interior walls, since the cabin orientation is not fixed.

As the cabin interior is relatively climate-controlled (i.e., maintains a temperature between $0°C \rightarrow 10°C$ in the winter), thermal effects could be neglected. Also, the remote location of the telescope meant that extraneous ground-based electromagnetic radiation did not require consideration.

III. ELECTRONICS RACK: DESIGN OVERVIEW

A. Model Overview

The SPT-SLIM electronics rack design, illustrated in Figure 5, consists of 2 columns. Each column has a width compliant with the EIA standard for 19-inch racks [8] and height allowing for storage of 24 rack units of electronics. Referencing Table I, the electronics total 33 rack units in height; thus, the rack contains adequate space. Protruding from opposing faces are the mounting rods, which attach to mounting bars at their ends. These serve as the mounting structures which will secure the electronics rack to the cabin walls.

The rack without electronics possesses a mass of about 156.6 kg. Its *main body* (i.e., rack without the mounting structures) has approximate dimensions of 45.95" × 44.42" × 30.04" and is primarily composed of aluminum T-slotted profiles as shown in Figure 6. Steel server rack rails, which the electronics are bolted to, attach to the vertical T-slotted profiles. The design also contains 2 eyebolts that will be necessary for lifting the rack into the SPT cabin. An aluminum sheet covers the top face to prevent miscellaneous falling objects (within the cabin) from damaging the electronics while also providing a useful work space. Refer to Appendix A for a complete list of parts used.

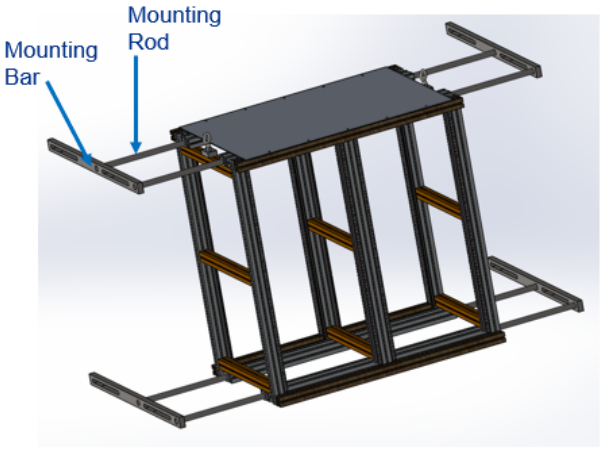

FIG. 5. SolidWorks model of SPT-SLIM electronics rack

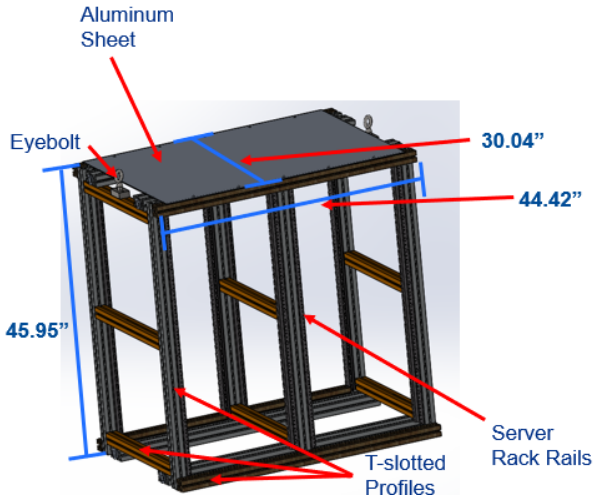

FIG. 6. *Main body* of SPT-SLIM electronics rack

The SPT-SLIM electronics rack closely models the SPT-3G electronics rack. The primary difference lies in the former having 2 columns, while the latter has 3. The SPT-SLIM electronics rack also has a slightly changed configuration of T-slotted profiles along with various dimensional differences.

B. T-Slotted Profiles and Server Rack Rails

2 models of aluminum T-slotted profiles were used in constructing the main body of the rack. The *4-slotted profile*, shown in Figure 7, and the *6-slotted profile*, shown in Figure 8, each possess a unique cross-sectional geometry which greatly simplifies the assembly process. In particular, the slots on each face, in combination with the specialized square nuts with position fixing listed in Table II (see Appendix A), allow for adjacent members to be connected without drilling holes—therefore lessening the amount of labor and time required. Furthermore, the presence of these slots allows for additional features (e.g., a third column) to be easily added to the electronics rack if necessary. This convenience is significant in the cramped environment of the SPT cabin.

Each steel server rack rail is 24 rack units (42") in length and possesses a flange having a row of 10-32 tapped holes, a face with 5 slots, and an additional L-shaped flange, as shown in Figure 9. These slots are bolted to the appropriate slot of a vertical 4-slotted profile, mating the 2 parts together as illustrated in Figure 10. This orients the rack rail flange containing 10-32 tapped holes such that it is perpendicular to the aforementioned slot of the 4-slotted profile. Corresponding threaded holes on opposing rack rail flanges (see Figure 10) are separated by 18.312" according to the EIA standard for 19" racks [8]. The various electronics are bolted to these pairs of holes and thus secured to the SPT-SLIM electronics rack.

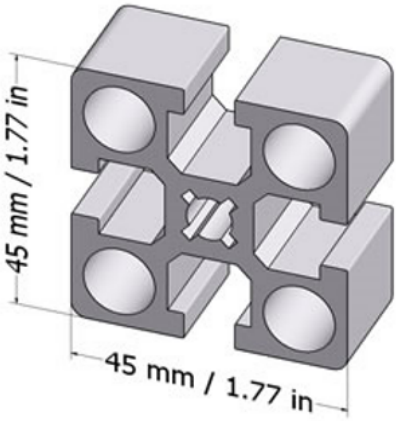

FIG. 7. 4-slotted profile [9]

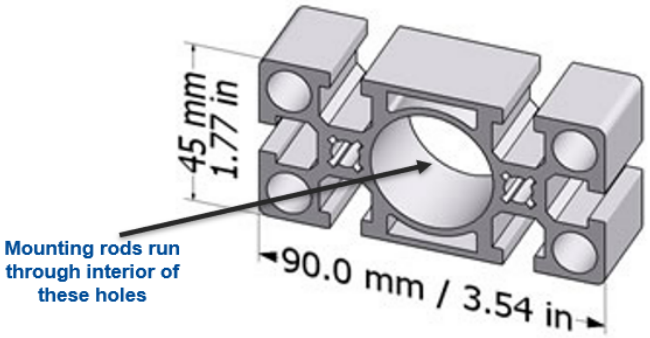

FIG. 8. 6-slotted profile [10]

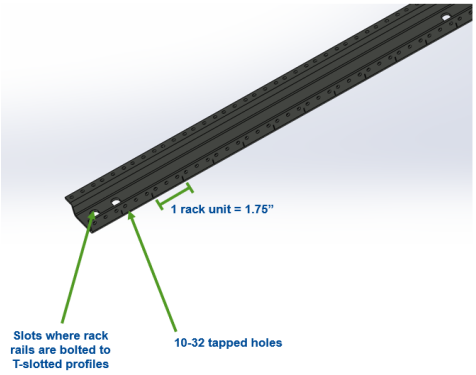

FIG. 9. SolidWorks model of server rack rail

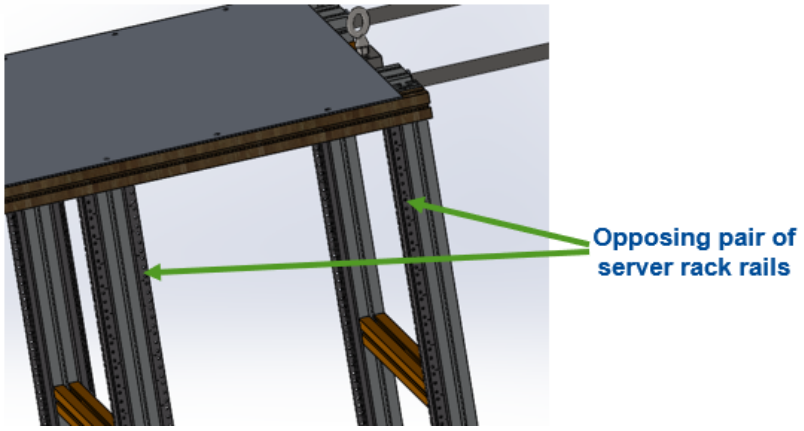

FIG. 10. Server rack rail bolted to vertical 4-slotted profiles in SPT-SLIM electronics rack

C. Mounting Scheme and Positioning Within SPT Cabin

The SPT-SLIM electronics rack will be attached to mounting plates offset from the SPT-3G cryostat in the positive r-direction, as indicated in Figure 12. These mounting plates are essentially extrusions in the cabin walls perpendicular to the ϕ direction and contain threaded holes. The mounting bars are bolted to these plates by overlapping the slots of the former with the holes of the latter, as depicted in Figure 11.

The mounting bars were specifically designed to be compatible with the mounting plate configuration and therefore needed to be custom-machined. Furthermore, they—along with the mounting rods—endure the greatest loads in this mounting scheme. Thus, AISI 304 stainless steel was chosen as the material for both parts in order to better preserve their structural integrity under the expected forces.

The implementation of slots in the mounting bar geometry allows for some flexibility in positioning the electronics rack within the cabin. Figures 11 and 12 both present the 2 extreme cases—labeled as the maximum and minimum offset positions. The former configuration maximizes the shortest distance (in the r-direction) between the electronics rack and SPT-3G cryostat; the latter configuration minimizes this same distance. Referencing Figures 13 and 14, this displacement is 17.20" for the maximum offset position and 9.38" for the minimum offset position. The SPT-SLIM electronics rack may be installed anywhere between these 2 extremal configurations, suggesting a variability in location of approximately 7.82". This freedom of translation only exists prior to mounting. Once this occurs, the rack is completely fixed with respect to the cabin.

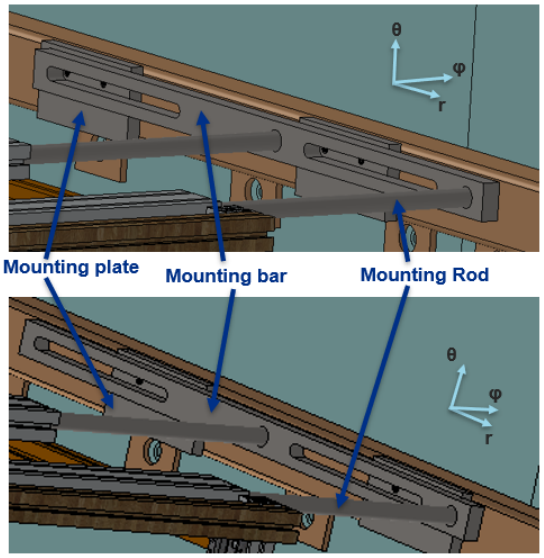

FIG. 11. Mounting bar in maximum (top image) and minimum (bottom image) offset positions

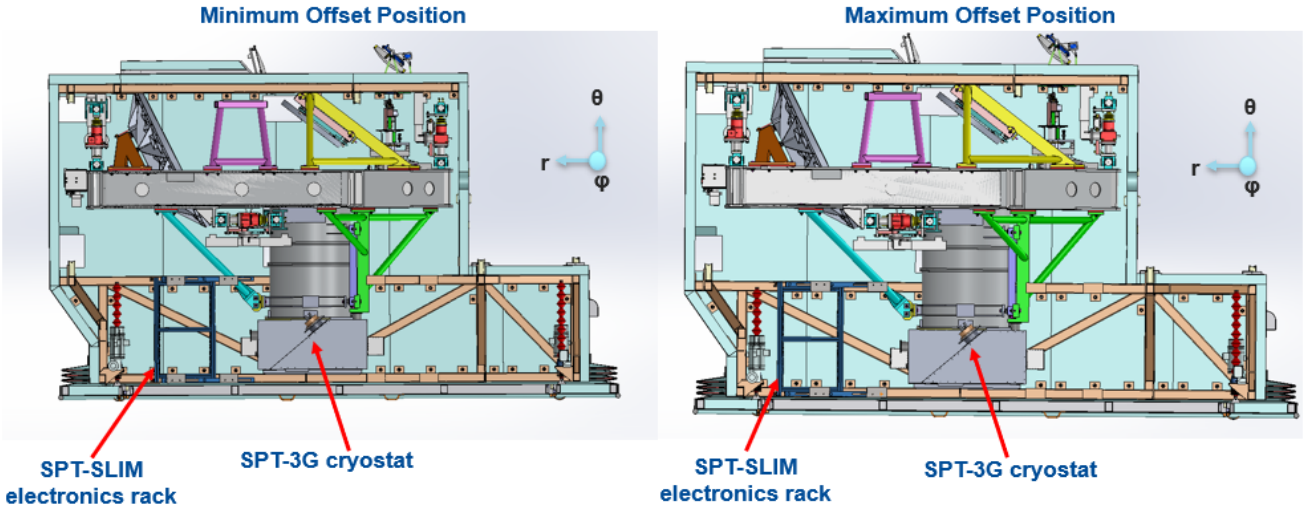

FIG. 12. Cross-sectional views of SPT cabin showing maximum (farthest from SPT-3G cryostat) and minimum (closest to SPT-3G cryostat) offset positions of SPT-SLIM electronics rack

D. Lifting Scheme

When the SPT cabin is docked, its floor (i.e., the face perpendicular to the θ-direction and containing points with minimal θ-values—see Figure 12) is permitted to open. This allows for objects to be lifted up (i.e., in the positive

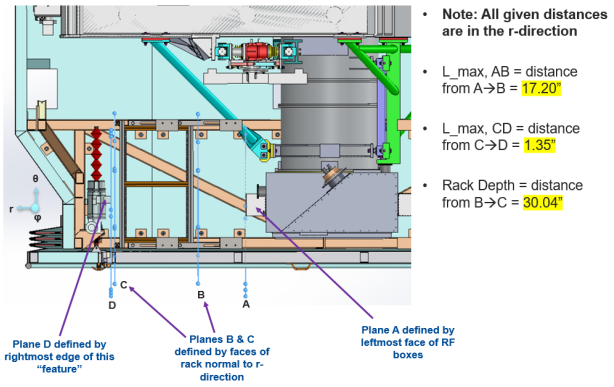

FIG. 13. Maximum Offset Position: SPT-SLIM electronics rack is offset from the RF box labeled plane A by approximately 17.20”

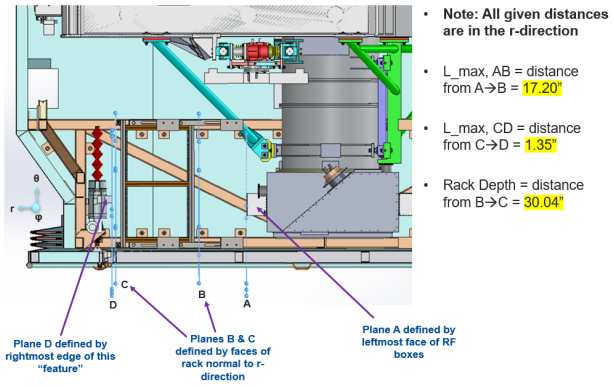

FIG. 14. Minimum Offset Position: SPT-SLIM electronics rack is offset from the RF box labeled plane A by approximately 9.38”

θ-direction) into the cabin interior. Executing this with the SPT-SLIM electronics rack and its housed components will not be a trivial matter, given their considerable combined mass of approximately 287.5 kg. Indicated in Figure 5, eyebolts were added to the design as a solution to this problem. Figure 15 depicts their role in the lifting scheme. Chain hoists will be attached to the eyebolts—which are fixed to the electronics rack. In addition, the hoists will be connected to lifting straps wrapped around the optics bench (see Figure 16). These can then be utilized to raise the electronics rack into the desired position and mount it.

The current plan is to carry out this strategy without the electronics bolted in to lessen the weight imposed on the optics bench. Once the rack is securely mounted and the chain hoists are removed, the electronics may be inserted. This method is less convenient but will ensure preservation of the optics bench’s structural integrity. This decision was not motivated by a concrete mathematical or engineering analysis but rather by rough estimates on the load-bearing ability of the optics bench. Thus, it may be worthwhile to more formally explore this topic in order to determine if such an approach is necessary.

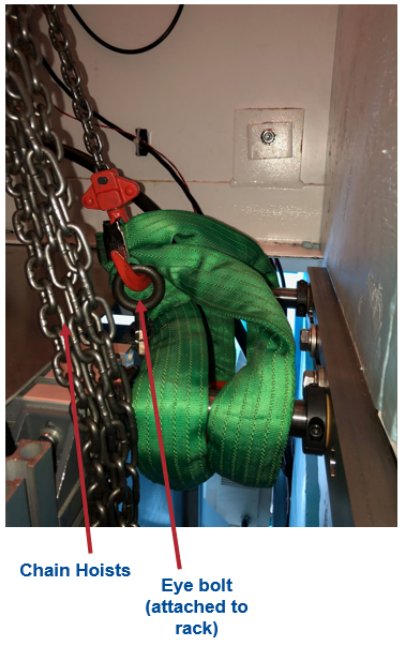

FIG. 15. Lifting apparatuses attached to electronics rack

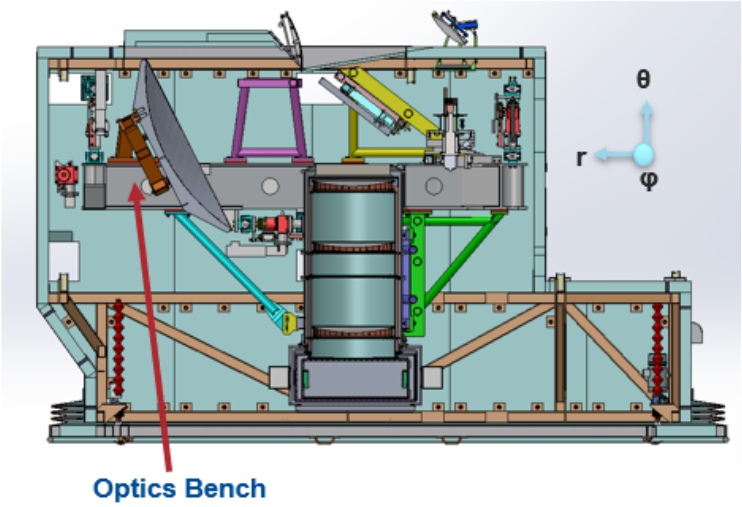

FIG. 16. Cross-section view of the SPT cabin indicating the location of the optics bench

IV. ELECTRONICS RACK: DESIGN TESTING

As the SPT-SLIM electronics rack and its stored electronics possess a significant combined mass ($\approx$ 287.5 kg), further analysis was necessary in order to confirm the capability of the design in supporting all expected loads.

A. Mounting Rod Deflection Calculation

While devising the mounting scheme, one of the primary concerns was whether the mounting rods would undergo non-elastic deformation. Thus, a simplified 1-D FEA was performed utilizing an online beam-deflection calculator to estimate the expected deflection in a single rod [5]. The combined mass of the rack and electronics—minus that of the 4 mounting rods themselves—was calculated to be 284.44 kg. This was divided equally amongst the rods, leading to a total weight of about 697.6 N imposed on each one. Furthermore, they were assumed to have a diameter of 25 mm, length of 2057.4 mm (81"), and Young's Modulus of 190 GPa—equivalent to that of AISI 304 stainless steel [2]. Note that some of these parameters (e.g., overall system mass, mounting rod length, and mounting rod diameter) do not reflect their current values. However, the differences are minute enough such that redoing the calculations with updated parameters was not necessary.

2 models were considered for the calculated load's application. The first was a worst-case scenario which imposed the weight as a point force located halfway along the rod's longitudinal axis and oriented perpendicularly to it. The second case considered this same weight to be a uniformly distributed force as crudely depicted in Figure 17.

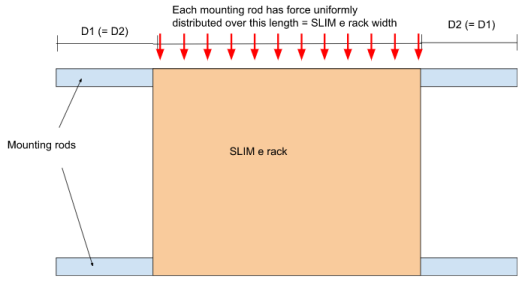

FIG. 17. Simple diagram detailing configuration used for 2nd (distributed load) case of mounting rod deflection computation

The first configuration produced magnitudes of 0.179 kNm, 0.349 kN, and 8.68 mm for the maximal bending moment, shear force, and shear deflection respectively. In the second case, these same quantities were discovered to be 0.161 kNm, 0.349 kN, and 6.79 mm. From the maximum shear force experienced ($F_{shear,max}$) and the cross-sectional area (A) of the rod, the maximum shear stress was obtained via $\tau_{max} = \frac{F_{shear,max}}{A}$. The von Mises yield criterion for pure shear stress, which states the relationship between shear (k) and tensile yield strength (σ) to be $k = \frac{\sigma}{\sqrt{3}}$ [13], was then applied. Given that AISI 304 stainless steel has a tensile yield strength of $\sigma_{\text{AISI, 304}} = 206.807$ MPa [2], both cases kept the mounting rod in the elastic deformation regime by a factor of safety (FOS) around 167.9. The presence of such a large FOS emphatically confirmed that the mounting rod could tolerate all required loads and therefore justified its application within the mounting scheme.

B. SolidWorks FEAs

Following completion of the SPT-SLIM electronics rack design, it became imperative to analyze its durability under expected loading conditions. Thus, static FEAs were performed within SolidWorks using the von Mises stress theory for multi-axial loading [13]. This was done initially for a single mounting bar in the maximum and minimum offset positions. It was later repeated for a simplified version of the electronics rack in both extremal positions and for multiple orientations of the cabin. For each model, 4 plots were generated, detailing von Mises stress, resultant displacement, equivalent strain, and FOS. Only 2—the resultant displacement and FOS plots—are included for the sake of brevity. The latter was defined according to the generalized von Mises yield criterion, which claims yielding to occur when the von Mises stress matches the tensile yield strength of the material [13]; thus, the FOS was set to be the latter divided by the former.

As mentioned above, the first study was performed on a mounting bar in both the maximum and minimum offset positions. The locations where they were bolted to the mounting plates were modeled as fixed supports, and vertical point loads were added to the circular holes which the mounting rods are inserted into—as shown in Figures 18 and 19. The magnitudes of these forces were all set to be about 352.6 N. This corresponds to equally distributing the combined mass of the rack and electronics ($\approx$ 287.5 kg) amongst the 8 points of contact between mounting rods and bars (i.e., the 2 circular holes found within each of the 4 mounting bars).

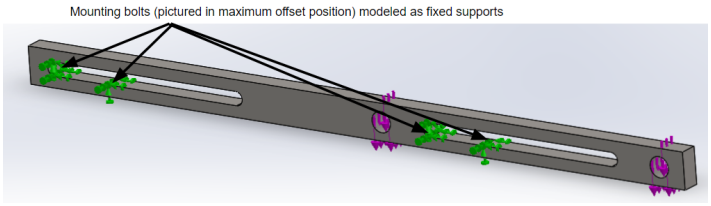

FIG. 18. Fixture and load positioning for mounting bar in maximum offset position

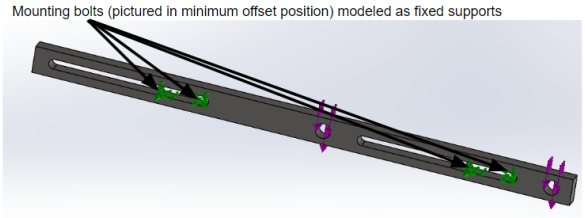

FIG. 19. Fixture and load positioning for mounting bar in minimum offset position

For the mounting bar in its maximum offset position, the greatest resultant displacement experienced was 0.256 mm, while the minimal FOS was 6.312—as depicted in Figures 20 and 21. When the bar was moved to its minimum offset position, these 2 quantities were computed to be 0.021 mm and 21.479 respectively, as illustrated in Figures 22 and 23.

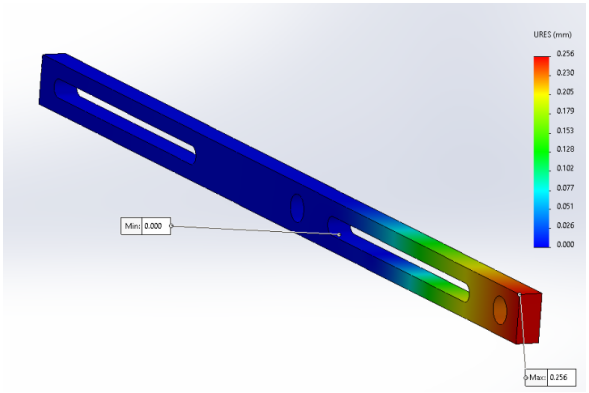

FIG. 20. Resultant displacement plot for mounting bar in maximum offset position

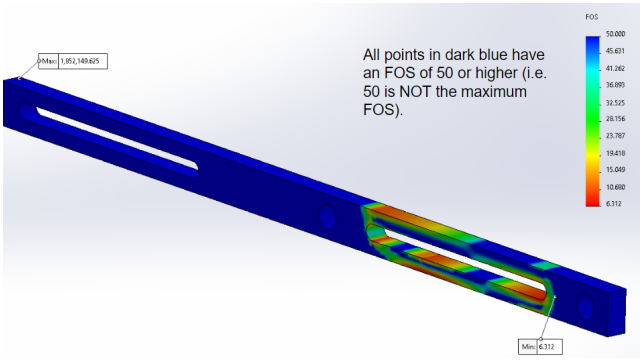

FIG. 21. FOS for mounting bar in maximum offset position

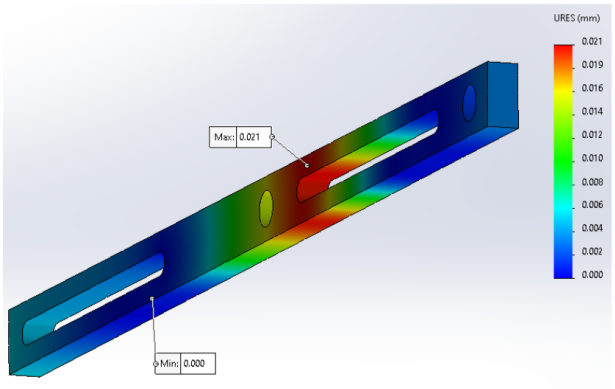

FIG. 22. Resultant displacement plot for mounting bar in minimum offset position

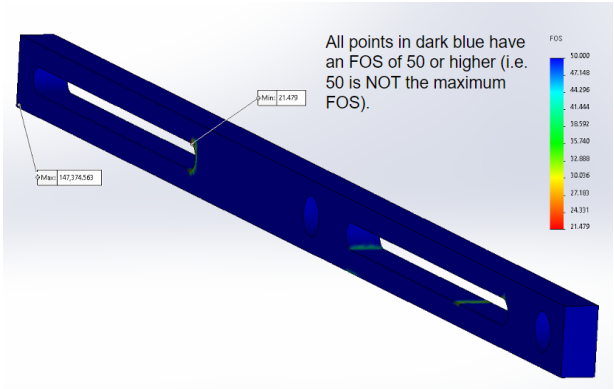

FIG. 23. FOS for mounting bar in minimum offset position

It was also desired to simulate loading conditions on the overall electronics rack model. However, this would have been unnecessarily time-intensive and computationally expensive due to the sheer number of parts in the assembly. Thus, a simplified version was created, as shown in Figures 24 and 25. This model preserved the mounting structures but replaced the main body with a solid block of the same size, as given in Figure 6. This block was assigned the material properties of Aluminum 6061, save for its density which was set to be about 222.5 kg/m^3. As a result, the simplified model mass matched that of the actual rack with electronics bolted in ($\approx$ 287.5 kg). The choice of Aluminum 6061 was motivated by the T-slotted profiles that predominantly compose the main body of the rack also being made of this material.

This simplified rack was studied in both the maximum and minimum offset positions. The locations where the mounting rods are inserted into the mounting bars and where the mounting bars are bolted to the mounting plates were set to be fixed supports—as shown in Figures 24 and 25. Furthermore, roller supports were added to the block faces perpendicular to the longitudinal axes of the rods. This replicated the clamping shaft collars (see Table II in Appendix A) preventing the main body of the rack from sliding along the mounting rods. Finally, a gravitational acceleration vector normal to the top face of the simplified rack (given by the red arrows in Figures 24-29) was imposed on the entire system. This reflects the orientation of the cabin when its floor is parallel to the surface of the Earth (e.g., when docked).

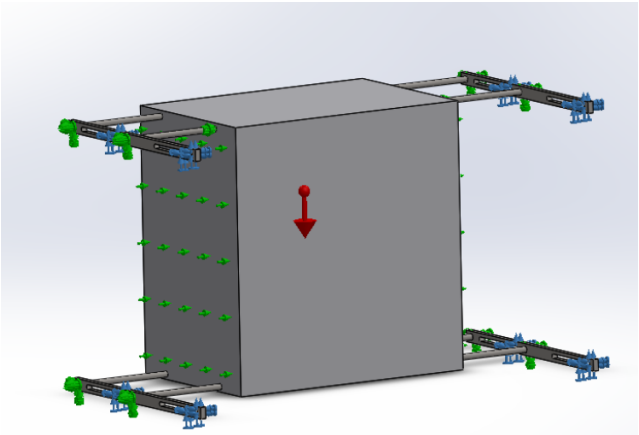

FIG. 24. Fixture positioning for simplified rack in maximum offset position and cabin at 0° elevation with respect to Earth's surface

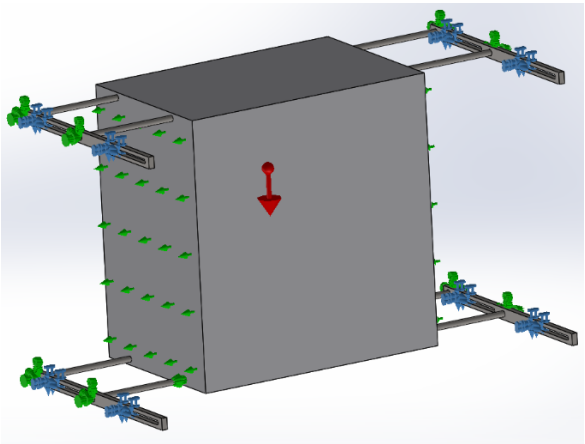

FIG. 25. Fixture positioning for simplified rack in minimum offset position and cabin at 0° elevation with respect to Earth's surface

For the maximum offset position, the greatest resultant displacement experienced by the simplified model was given to be 0.407 mm, and the smallest FOS was 10.48—as shown in Figures 26 and 27. Referencing Figures 28 and 29, the mimimum offset position resulted in corresponding extrema of 0.549 mm and 5.3 respectively.

The final iteration of testing involved changing the orientation of the gravitational acceleration vector (given by red arrows in Figures 30-33) such that it was at a 45° angle relative to the top surface of the simplified rack. This choice reflects the orientation of the cabin that approximately corresponds to the primary elevation angle which SPT-SLIM will observe at. Once again, the simulation was run for the rack in the maximum and minimum offset positions—with the fixture configurations matching their counterparts depicted in Figures 24 and 25. The maximum offset position exhibited resultant displacements no greater than 0.407 mm and an FOS no smaller than 10.838, as conveyed by Figures 30 and 31. The minimum offset position yielded 0.549 mm and 4.931 respectively for these 2 values, as detailed in Figure 32 and Figure 33.

C. Conclusions

Every method of testing maintained the mounting structures within the elastic deformation regime by at least an FOS of 4.931 and kept their deflections on the order of less than 1 cm. The SolidWorks FEAs—which more accurately model the true design—never had deflections above 1 mm. Thus, there exists a significant margin for error in terms of underestimating load application, allowing for a confident assertion that the mounting scheme will not undergo

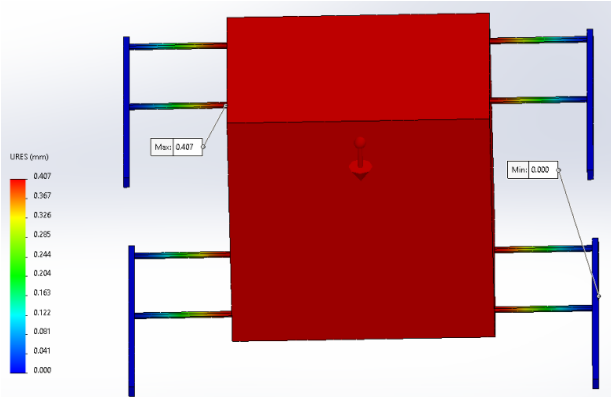

FIG. 26. Resultant displacement plot for simplified rack in maximum offset position and cabin at 0° elevation with respect to Earth's surface

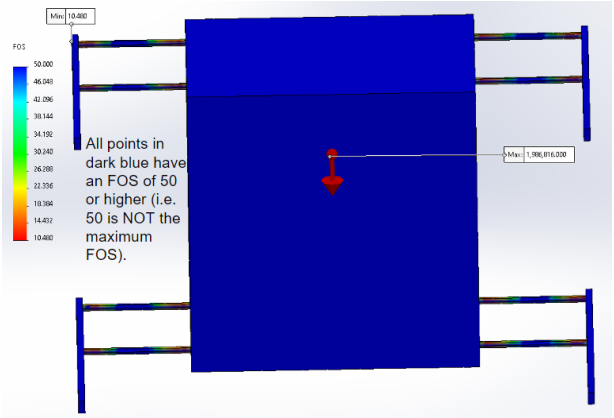

FIG. 27. FOS plot for simplified rack in maximum offset position and cabin at 0° elevation with respect to Earth's surface

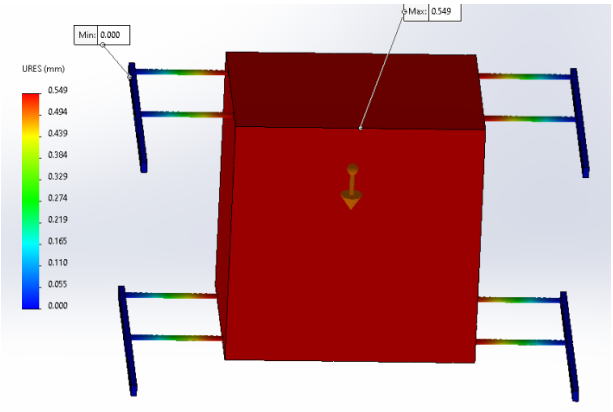

FIG. 28. Resultant displacement plot for simplified rack in minimum offset position and cabin at 0° elevation with respect to Earth's surface

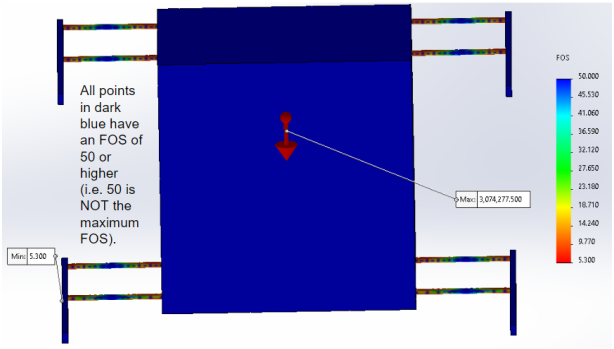

FIG. 29. FOS plot for simplified rack in minimum offset position and cabin at 0° elevation with respect to Earth's surface

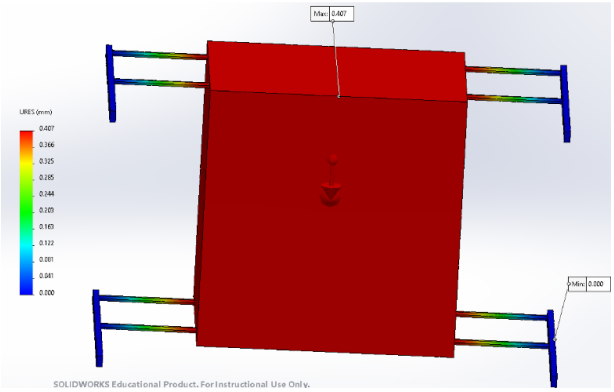

FIG. 30. Resultant displacement plot for simplified rack in maximum offset position and cabin at 45° elevation with respect to Earth's surface

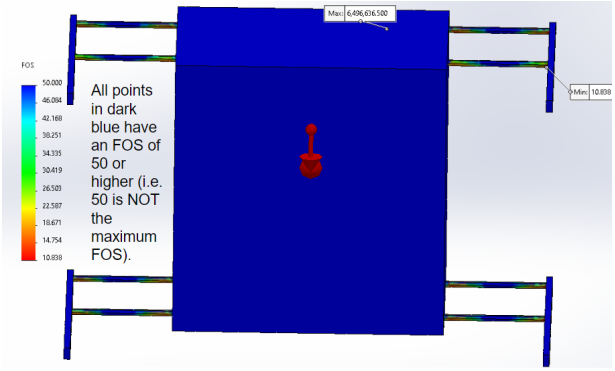

FIG. 31. FOS plot for simplified rack in maximum offset position and cabin at 45° elevation with respect to Earth's surface

plastic deformation or fracturing. Furthermore, the parts chosen for the main body of the rack are all rated for much greater forces than anything that will be experienced within the cabin. Finally, the close resemblance between the SPT-SLIM electronics rack and its SPT-3G counterpart instills confidence that the former will not fail. The latter is

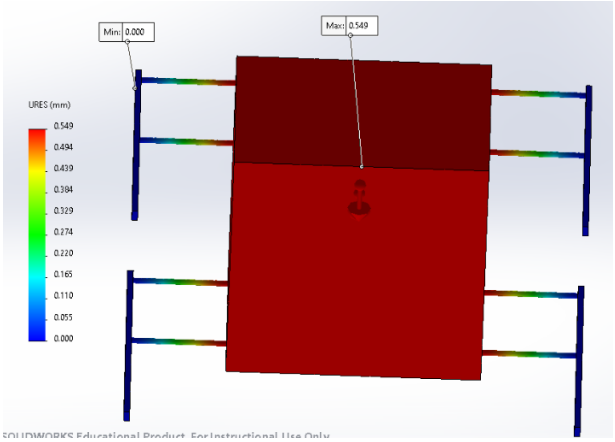

FIG. 32. Resultant displacement plot for simplified rack in minimum offset position and cabin at 45° elevation with respect to Earth's surface

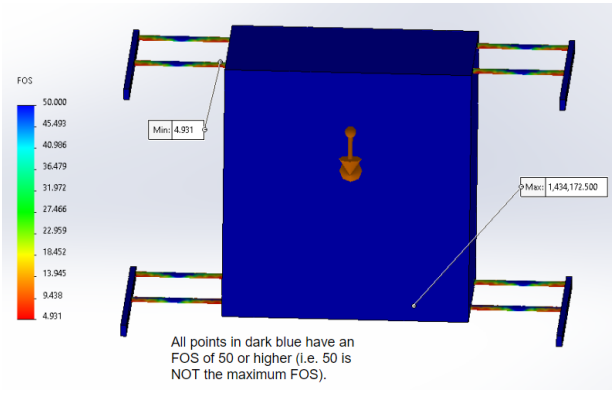

FIG. 33. FOS plot for simplified rack in minimum offset position and cabin at 45° elevation with respect to Earth's surface

currently installed within the cabin and has not exhibited any mechanical shortcomings. Thus, it is fair to assume that the SPT-SLIM rack, which supports less weight and is more compact, will enjoy similar success. These 3 statements combine to justify the claim that the SPT-SLIM electronics rack should be able to handle any loads it may encounter within the cabin.

V. ELECTRONICS RACK: PROJECT STATUS AND NEXT STEPS

As illustrated above, the electronics rack design has been finalized and validated. Parts have been ordered and should reach Fermilab by the end of August 2022. Also, there will potentially be a test deployment and installation at SPT this upcoming austral summer. This would serve as a valuable confirmation that the design truly does satisfy the claims provided above. The electronics rack will then be redeployed with the rest of the SPT-SLIM instrumentation just prior to or at the beginning of the 2023-2024 austral summer [7].

VI. SPT-SLIM DETECTOR FORECASTING

Understanding the signal-to-noise ratio (SNR) for a system of detectors is critical to data measurement and uncertainty prediction. An older instrument model, shown in Figure 34, currently exists for SPT-SLIM [7]. Since its inception though, numerous experimental parameters have changed. This includes influential factors such as the survey size, optical configuration, detector distribution within the focal plane, pixel size, illumination pattern of pixels on the SPT-SLIM mirrors, angular resolution, temperatures of the various optical surfaces, and many more. These factors have contributed to changes in variables such as the noise equivalent temperature (NET), which is related to the noise power spectrum [4].

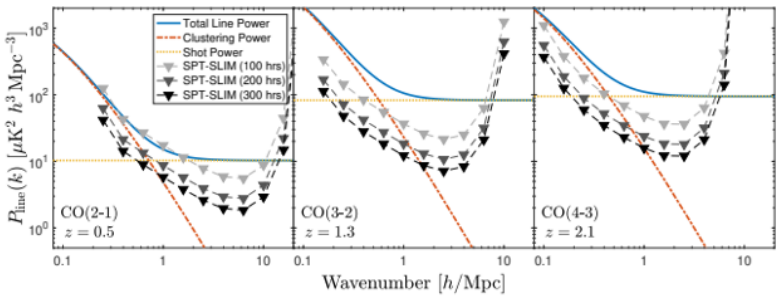

FIG. 34. Plots of signal and noise power spectra produced via an older and outdated instrument model [7]

The current ambition is to revise the existing model for the noise power spectrum. Significant progress has been made towards this goal, as multiple contributing terms have been coded within Python. However, this objective will not be completed by the end of the 2022 SIST internship. Future steps involve completing the Python code for the entirety of the noise power spectrum and then doing the same for the signal spectrum–such that an updated version of Figure 34 may be created.

ACKNOWLEDGEMENTS

I would like to thank Adam Anderson and the rest of the SPT collaboration for their immense help, patience, and kindness. I would also like to express gratitude towards my SIST mentors, Ahmed Syed and Alex Drlica-Wagner, along with my fellow Group 4 interns, for their guidance and feedback. Finally, I am grateful to the SIST internship committee for their efforts in providing this wonderful opportunity.

REFERENCES

[1] Anderson, A. J., *Technology for SPT-SLIM and Line-Intensity Mapping*, APS April Meeting (2022).

[2] Davis, J. R., *Metals Handbook Desk Edition*, ASM International (1998).

[3] Dibert, K., Barry, P., Pan, Z., et al., *Development of MKIDs for Measurement of the Cosmic Microwave Background with the South Pole Telescope*, J Low Temp Phys (2022) [arXiv:2111.04816].

[4] Dizgah, A. M., Keating, G. K., Karkare, K. S., et al., Astrophys. J. **926**, no.2, 137 (2022) [arXiv:2110.00014].

[5] *Free Beam Calculator*, ClearCalcs (2021). `https://clearcalcs.com/freetools/beam-analysis/us`

[6] Furlanetto, S. R., Bowman, J. D., Mirocha, J., et al., arXiv e-prints, arXiv:1903.06212 (2019).

[7] Karkare, K. S., Anderson, A. J., Barry, P. S., et al., *SPT-SLIM: A Line Intensity Mapping Pathfinder for the South Pole Telescope*, J Low Temp Phys (2022) [arXiv:2111.04631].

[8] *19-inch rack*, Wikipedia (2022). `https://en.wikipedia.org/wiki/19-inch_rack`

[9] *Profile 45×45*, MiniTec (2017). `http://www.minitecframing.com/Products/Aluminum_Profiles/Aluminum_Profile_Catalog_Pages/20.1006_Aluminum_Profile_45x45.html`

[10] *Profile 45×90 S*, MiniTec (2017). `https://www.minitecframing.com/Products/Aluminum_Profiles/Aluminum_Profile_Catalog_Pages/20.1017_Profile_45x90S.html`

[11] Sobrin J. A., Anderson, A. J., Bender, A. N., et al., Astrophys. J. Supp. **258**, no.2, 42 (2022) [arXiv:2106.11202].

[12] *South Pole Telescope*, Wikipedia (2022). `https://en.wikipedia.org/wiki/South_Pole_Telescope`

[13] *von Mises yield criterion*, Wikipedia (2022). `https://en.wikipedia.org/wiki/Von_Mises_yield_criterion`

APPENDIX A: PARTS LIST

Table II contains all the parts necessary for the fabrication of the SPT-SLIM electronics rack. Also included is a list of brief descriptions for all parts.

Part Name	Vendor Name	Part Number	Custom Dim.	Qty.
Profile 45 × 45	MiniTec	20.1006	45.82"[a]	6
Profile 45 × 45	MiniTec	20.1006	44.42296"[a]	4
Profile 45 × 45	MiniTec	20.1006	22.95669"[a]	9
Profile 45 × 90 S	MiniTec	20.1017	44.42"[a]	4
Server Rack Rail	Hammond	CCR42TZPL	24u = 42"[a]	8
M8×16 Socket Head Cap Screw[b]	MiniTec	21.1200	N/A	50
M8 Square Nut with Position Fixing[b]	MiniTec	21.1351/2	N/A	54
M8 Metric Oversized Steel Washer	McMaster	96505A116	N//A	54
Mounting Bar[c]	Protolabs	N/A	N/A	4
1" Diameter Multipurpose 304/304L Stainless Steel Rod	McMaster	4011N24	79.5"	4
Extreme Strength Grade 9 Steel Hex Head $\frac{1}{2}$-13 UNC Screw	McMaster	90201A418/90201A423	1.5"/1.75"[d]	16
Zinc Yellow-Chromate Plated Grade 9 Steel Washer	McMaster	90850A300	N/A	18
Angle 45 GD-Z with Position Fixing Nuts	Minitec	21.1349/7	N/A	68
Inner Collar/Spacer[c]	Protolabs	N/A	N/A	8
Black-Oxide 1215 Carbon Steel Clamping Shaft Collar	McMaster	6435K18	N/A	16
Steel Eyebolt with Shoulder - for Lifting	McMaster	3014T491	N/A	2
Extreme-Strength Steel Hex Nuts-Grade 9	McMaster	95036A024	N/A	2
Eyebolt Plate[c]	Protolabs	N/A	N/A	2
M8×40 Socket Head Cap Screw[b]	MiniTec	21.1210	N/A	4
$\frac{1}{8}$"-Thick Aluminum 3003 Mill Finish Sheet Metal	MiniTec	21.9523	40.88" x 30.04"[e]	1
Swivel Caster 5" with Top Plate and Brake	MiniTec	21.9404	N/A	6

[a] Length
[b] Thread pitch = 1.25mm
[c] Custom-machined
[d] Threaded length (either choice viable)
[e] Sheet dimensions

TABLE II. Parts list for SPT-SLIM electronics rack

- **Profile 45 × 45**:
  - **45.82" length**: Gray-colored (in Figure 5) aluminum 4-slotted profile which server rack rail attaches to (see Figure 10). Refer to section III B for further details.
  - **44.42296" length**: Dark brown-colored (in Figure 5) aluminum 4-slotted profile parallel to mounting rods. Refer to section III B for further details.
  - **22.95669" length**: Bronze-colored (in Figure 5) aluminum 4-slotted profile perpendicular to mounting rods (see Figure 5). Refer to section III B for further details.
- **Profile 45 × 90 S**: Gray-colored (in Figure 5) aluminum 6-slotted profile which is coaxial with its corresponding mounting rod (see Figure 8). Refer to section III B for further details.
- **Server Rack Rail**: Specialized steel rail which SPT-SLIM electronics are bolted to (see Figures 9 and 10). Refer to section III B for further details.
- **M8×16 Socket Head Cap Screw**: Used to bolt server rack rails to vertical 4-slotted profiles (see Figure 10) and attach aluminum sheet metal to top face of electronics rack (see Figure 5).
- **M8 Square Nut with Position Fixing**: Specialized nut which can be securely fitted within slots of T-slotted profiles.
- **M8 Metric Oversized Steel Washer**: Washer possessing an oversized outer diameter that can be used with M8 screws.

- **Mounting Bar**: Custom-machined AISI 304 stainless steel bar that is mounted to an SPT cabin wall and therefore fixes the electronics rack's position within the cabin (see Figures 5 and 11). Refer to III C for further details.
- **1" Diameter Multipurpose 304/304L Stainless Steel Rod**: Mounting rod which connects the main body of the rack to the mounting bars (see Figures 5 and 11). Refer to section III C for further details.
- **Extreme Strength Grade 9 Steel Hex Head $\frac{1}{2}$-13 UNC Screw**: Used to bolt the mounting bars to the mounting plates (see Figure 11).
- **Zinc Yellow-Chromate Plated Grade 9 Steel Washer**: Washer used with $\frac{1}{2}$-13 screw.
- **Angle 45 GD-Z with Position Fixing Nuts**: Angle-shaped bracket that connects adjacent T-slotted profiles at 90° angles.
- **Inner Collar/Spacer**: Aluminum spacer between the mounting rods and the interior surface of the central hole in the 6-slotted profile (see Figure 8).
- **Black-Oxide 1215 Carbon Steel Clamping Shaft Collar**: Specialized collars located on mounting rods that are meant to prevent the mounting bars and main body of the electronics rack from translating along the rods.
- **Steel Eyebolt with Shoulder - for Lifting**: Specialized bolts secured to the electronics rack that are designed to assist with lifting heavy loads (see Figure 15). Refer to section III D for further details.
- **Extreme-Strength Steel Hex Nuts-Grade 9**: Nuts designed to pair with $\frac{1}{2}$-13 screws.
- **Eyebolt Plate**: Custom-machined AISI 304 stainless steel block which connects appropriate bronze-colored T-slotted profiles to an eyebolt (see Figure 5).
- **M8×40 Socket Head Cap Screw**: Used to bolt eye bolt plates to the electronics rack.
- **$\frac{1}{8}$"-Thick Aluminum 3003 Mill Finish Sheet Metal**: Metal sheet covering the top face of the electronics rack (see Figure 5).
- **Swivel Caster 5" with Top Plate and Brake**: Caster and wheel system which can be added to the electronic rack in order to significantly ease transportation when not mounted to the cabin.